Arab J Geosci (2017) 10: 8
DOI 10.1007/s12517-016-2790-2

ORIGINAL PAPER

Hydrochemistry and gas geochemistry of the northeastern Algerian geothermal waters

M. Belhai[1] · **Y. Fujimitsu**[2] · **J. Nishijima**[2] · **M. Bersi**[3]

Received: 16 January 2016 / Accepted: 5 December 2016 / Published online: 28 December 2016

Abstract This study focuses on the water and gas chemistry of the northeastern Algerian thermal waters. The helium gas was used to detect the origin of the geothermal fluid. In the Guelma Basin, the heat flow map shows an anomaly of 120 ± 20 mW/m^2 linked to the highly conductive Triassic extrusion. The chemical database reveals the existence of three water types, Ca-SO_4/Na-Cl, which are related to evaporites and rich in halite and gypsum minerals. The third type is Ca (Na)-HCO_3, which mostly characterizes the carbonated Tellian sector. The origin of thermal waters using a gas-mixing model indicates a meteoric origin, except for the El Biban hot spring (W10), which shows a He/Ar ratio of 0.213, thus suggesting the presence of batholith. The helium distribution map indicates a lower ^{3}He/^{4}He ratio between 0 Ra and 0.04 Ra in the W10 and W15 samples, which is compatible with the crustal ratio. Reservoir temperatures estimated by silica geothermometers give temperatures less than 133 °C. The geothermal conceptual model suggests that a geothermal system was developed by the deep penetration of infiltrated cold waters to a depth of 2.5 km and then heated by a conductive heat source (batholith for El Biban case). The thermal waters rise up to the surface through the deep-seated fractures. During their ascension, they are mixed with shallow cold groundwater, which increase the Mg content and cause the immature classification of the water samples.

Keywords Northeastern Algeria · Geothermal waters · Gas chemistry · Geothermometry · Conceptual model

✉ M. Belhai
mkhader89@gmail.com

[1] Department of Earth Resources Engineering, Graduate School of Engineering, Kyushu University, Fukuoka 819-0395, Japan

[2] Department of Earth Resources Engineering, Faculty of Engineering, Kyushu University, Fukuoka 819-0395, Japan

[3] Department of Geophysics, Faculty of Earth Sciences, Geography and Territorial Planning, Houari Boumediene University of Sciences and Technology, BP 32, Al Alia, 16111 Algiers, Algeria

Introduction

More than 70 principal hot springs are located in northeastern Algeria, and they have a temperature discharge ranging between 31 and 97 °C. Most of the geothermal waters have been used therapeutically for balneology since the Roman period. The hydrogeochemistry of the geothermal water discharge is strongly controlled by the host lithology (Issaadi 1992; Bouchareb-Haouchine 1993; Kedaid and Mesbah 1996; Saibi 2009).

The origin of the geothermal manifestations could be linked to the Mio-Plio-Quaternary magmatic events (Verdeil 1982) and a relatively high geothermal gradient that exists in northeastern Algeria (approximately 4.32 °C/100 m; Bouchareb-Haouchine 2012). This study focuses on the water chemistry and key source rocks to understand the interactions with the host rock. Gas species (Rezig and Marty 1995) are used to ascertain the origin of the different thermal manifestations using several gas ratios to estimate the geothermal reservoir temperature with gas geothermometry techniques.

Finally, the ^{3}He/^{4}He ratio variation and distribution map are used to examine the eventual intrusion at depth and to develop a geothermal conceptual model for northeastern Algeria (Fig. 1).

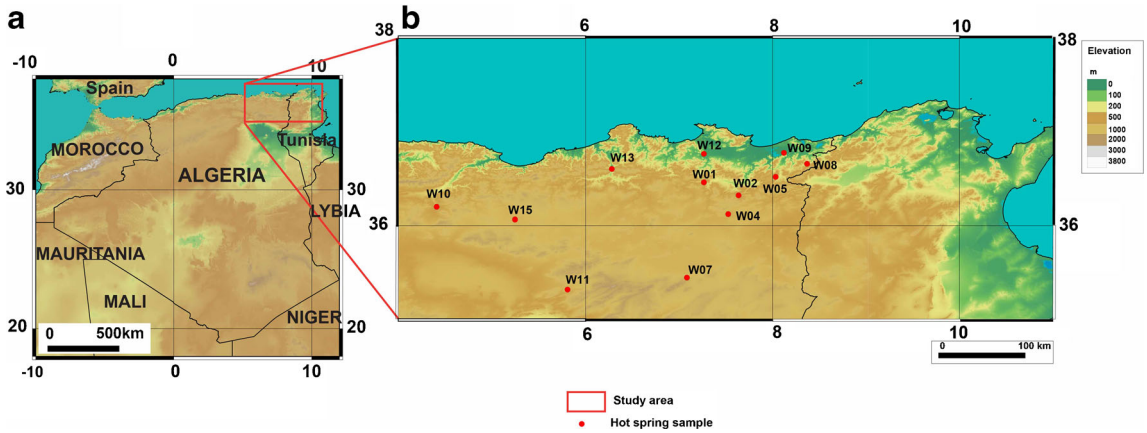

Fig. 1 **a** Study area in the northeastern part of Algeria. **b** With the location of the hot spring sampling points (in *red circles*)

Geological setting

The northeastern part of Algeria presents a complex geological setting that belongs to the North African margin as a part of the Maghrebide-Alpine belt (Fig. 2), which extends from Gibraltar to Sicily-Calabria (Domzig et al. 2006; Auboin and Durand-Delga 1971). The study area is situated in the external zones within the Tellian zones (Wildi 1983) and is mainly characterized by Miocene folds and *nappes* thrusted over the Atlasic foreland toward the south. The Atlasic domain consists of large-scale SW-NE anticlines and synclines that are crossed by SE graben and horst developed during the late Cretaceous collision between the African and European plates. These structures are inherited from the Eocene tectonic phase. The Atlasic domain is composed of a carbonated fossiliferous sequence that includes clays, gypsum, and secondary dolomites of Mesozoic to Eocene age. Certain E-W lineament trends compatible with deep E-W faults are abundant toward the southern part (Guiraud 1970). NE-SW trending faults facilitate the release and effusion of saline Triassic evaporites, thereby contributing to the surmounting *diapir zone*, which is typically expressed by gypsum, halite, and anhydrite of upper Triassic age. Toward the north and separating the external to the internal zones, the Numidian flysch domain, which was formed during the upper Miocene compressive phase, appears. It

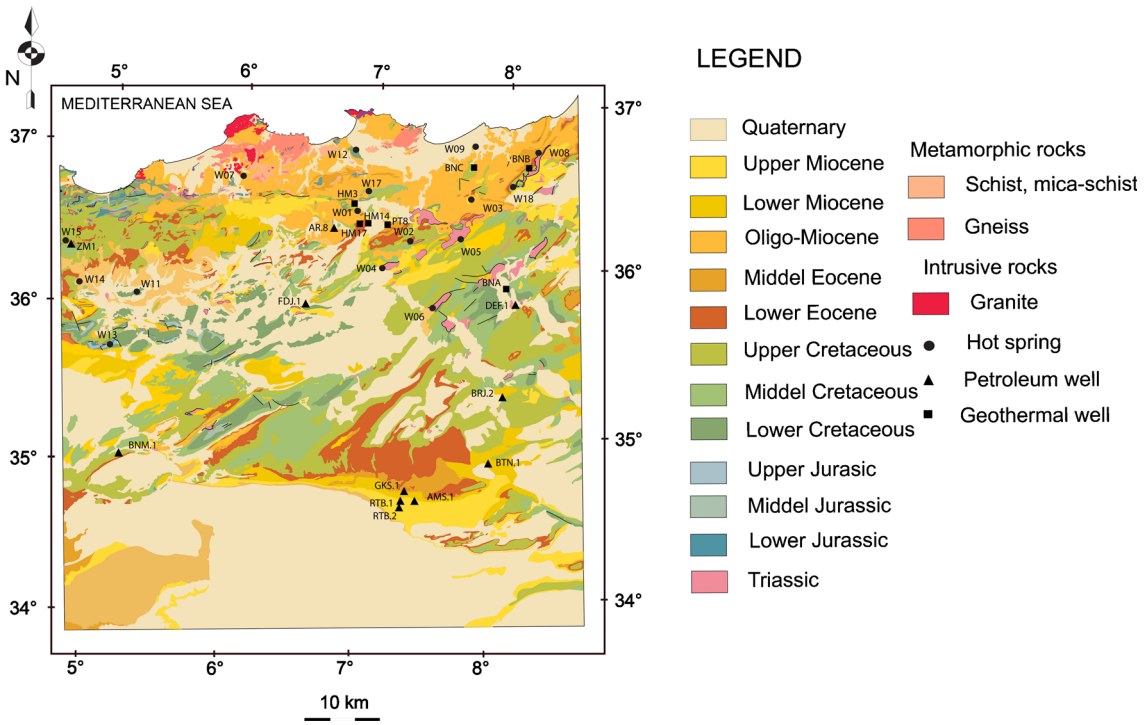

Fig. 2 Geological map of the different lithologies of the northeastern Algeria modified from Gouskov and Laffitte (1951)

is essentially composed of a thick alternating series of sandstones and clays of Oligo-Miocene age. The internal zones of the belt are located along the coast and form discontinuous massives that are considered a separation of part of the ancient Tethyan ocean (*AlKaPeCa*) from the European plate in the Early to Middle Miocene (Domzig et al. 2006). In the northeastern part of Algeria, a Hercynian metamorphic basement comprises the internal zones of the Magrebides belt and is covered by an essentially carbonated sequence of so-called "Dorsale-calcaire" (Durand-Delga 1969). Granitic and eruptive rocks are widespread in the coastal areas, which are dated from 9.3 to 24 Ma (Rezig and Marty 1995). Mineral deposits of Pb, Zn, Cu, Fe, and Hg and the higher geothermal gradients could be related to this Mio-Pliocene magmatic event, which resulted from the extensional phase of deformation. However, evidence of the southernmost intrusion of this magmatism and the crust melting process is still lacking.

Heat flow and tectonics

The heat flow map at the ground surface in the northeastern Algeria (Fig. 3) was estimated using temperature measurements from 38 petroleum and geothermal wells (Rezig 1991). This heat flow distribution map indicates important variations that are overprinted by short-wavelength anomalies.

Northward, the Guelma Basin (near W01, W02, and W04 in Fig. 3) shows high heat flow anomaly values varying between 80 and 120 ± 20 mW/m^2. Toward the south, a heat flow of 45 mW/m^2 is found (Rezig and Marty 1995).

This anomaly is exclusively linked to the local geological structures that belong to the Tellian sector, especially the Triassic evaporites and salt deposits that form NE-SW trending *diapir zones*, which extend from Bizerte (Tunisia) to Souk-Ahrass and Guelma (Algeria). In fact, salt has a thermal conductivity that is two to four times greater than that of other

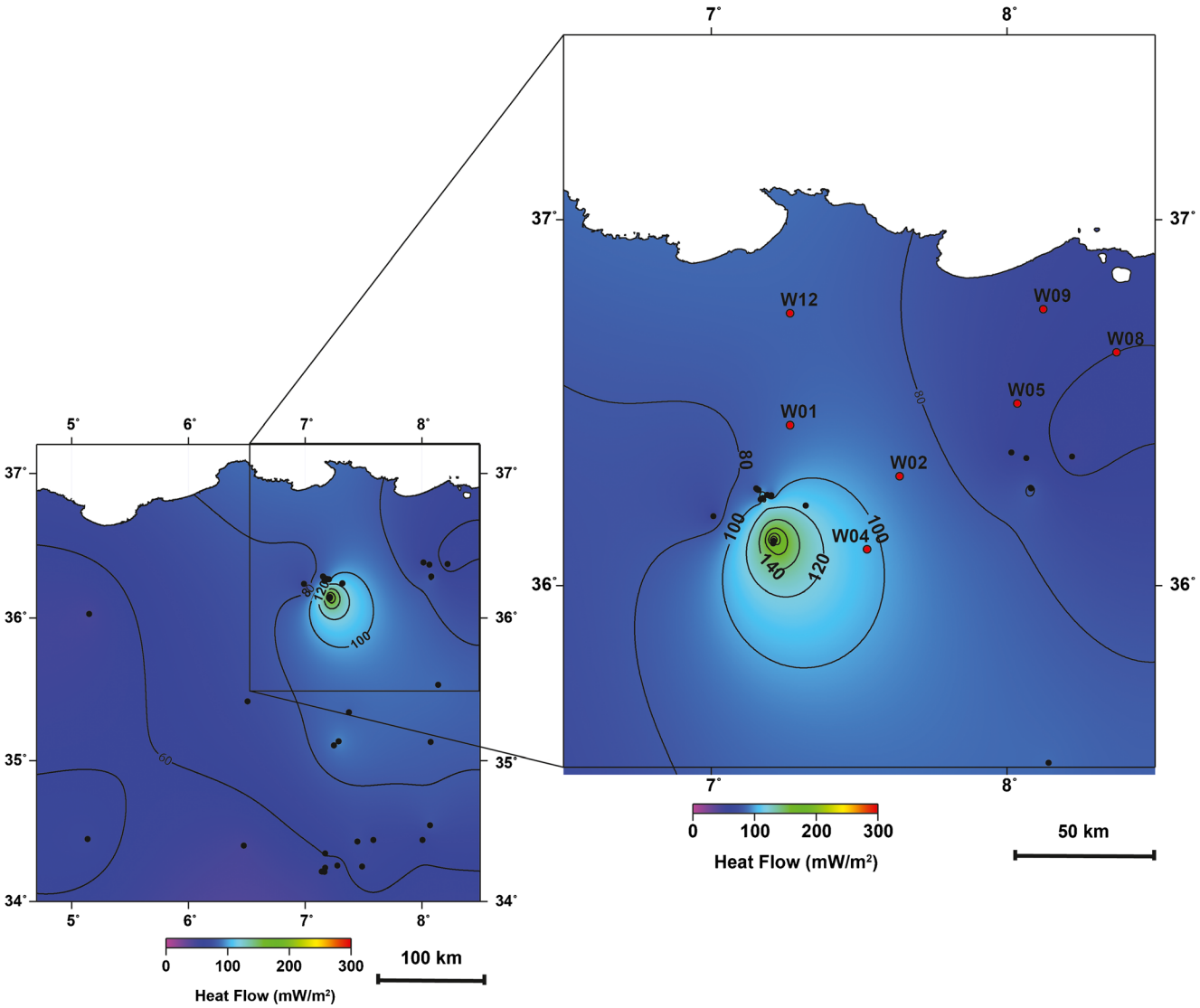

Fig. 3 Heat flow distribution map of northeastern Algeria determined from petroleum and geothermal wells

sedimentary rocks. Its values can be as high as 5 to 6 W m^{-1} K^{-1} (Cermak and Rybach 1982; Lerche and O'Brien 1987). Therefore, a salt diapir intruded in the sediment of much lower thermal conductivity will act as a conduit for heat transport, both vertically and horizontally (Magri et al. 2008). The presence of extensional Miocene-Pliocene-Quaternary volcanism in the internal zones of the North African plate border suggests a possible contribution of a recent mantle thermal event.

It is not clear in Fig. 3, but generally, in the northern part of Algeria, the heat flow distribution map shows an E-W trending anomaly that affects the northern part of the African plate, stretching from the Canaries (volcanic islands) to Libya (Saibi 2009).

Sampling and analysis methods

Rezig and Marty (1995) sampled 12 free and dissolved gases from hot springs in the northeastern Algeria. The sampled gases were evacuated in sealed glass tubes connected to a funnel.

The analyses were conducted at the M.A.G.I.E. Laboratory (University P. and M. Curie in Paris, France) using a mass spectrometer after both extraction and separation. The analytical uncertainties were estimated to be between ±5 and ±10% for the gas composition. Helium isotopic analyses were performed using a mass spectrometer with a magnetic sector, model V.G. 5400.

Major ion analyses (for Na^+, K^+, Ca^{2+}, Mg^{2+}, and SiO_2) were measured by atomic absorption spectrophotometry, while SO_4^{2-} concentrations were determined by spectrophotometry and alkalinity was determined using standard titration techniques. Cl^- was analyzed using the $AgNO_3$ titration method by ENEL (1982). For SiO_2 analysis, samples were diluted tenfold using deionized water to prevent SiO_2 precipitation in the water. SiO_2 concentrations were determined by atomic absorption spectrophotometry.

Results

Water chemistry

The discharge temperature, pH, and chemical composition of the collected water samples are reported in Table 1. Previous silica data were inferred from the database of each hot spring in order to estimate the reservoir temperatures (ENEL 1982; Kedaid 2007). The geothermal waters generally show a near neutral pH that ranges from 6.5 to 7.8 and are characterized by very high total dissolved solid (TDS) values up to 16,108 mg/L. This high water salinity is expected to be due to the interaction of the infiltrated meteoric waters with the saline host rocks and probably reflects a longer circulation and residence time.

According to the ternary diagrams (Fig. 4a, b), the northeastern Algerian geothermal waters can be classified into three major types. The majority of the collected water samples are sulfate waters with higher Ca-SO_4 contents (W17, W06, W07,

Table 1 Chemical composition (mg/L) of collected hot springs of northeastern Algeria (ENEL 1982; Kedaid 2007)

Sample ID	Hot spring (prefecture)	*T* (°C)	pH	TDS	Na^+	K^+	Mg^{2+}	Ca^{2+}	Cl^-	SO_4^{2-}	HCO_3^-	SiO_2
W01	H. Chellala (Guelma)	98	ND	1600	219	16	28	215	336	396	331	75
W02	H. N'Bails (Guelma)	34	6.6	6211	1550	12	157	370	2425	450	702	30
W03	H. Zaid	39	7.1	1302	128	6	91	145	330	43	580	22
W04	H. Ben Hachani (Sedrata)	71	6.8	2046	93	12	108	380	195	863	415	60
W05	H. Beni Salah (Guelma)	48	7.8	1256	358	8	28	23	295	30	592	55
W06	H. El-Hamma	34	7.6	2094	100	12	90	470	175	1150	320	14
W07	H. Salhine (Skikda)	55	6.5	2046	33	12	352	64	195	863	415	ND
W08	H. Meksa (El Kala)	36	6.9	704	75	8	60	64	135	48	360	39
W09	H. Sidi Djaballah	37	7.1	1262	273	10	61	50	350	150	427	33
W10	H. El Biban	80	7.8	16,108	5000	13	155	408	8300	1000	250	ND
W11	H. Soukhna	50	7.1	2052	413	4	82	124	775	283	260	ND
W12	H. El-Hamma-2	ND	ND	ND	60	3	82	124	775	283	260	ND
W13	H. Beni Haroune	42	7.3	3762	940	35	44	190	1688	375	244	ND
W14	H. Boutaleb (Setif)	52	7.1	3416	625	35	112	286	1175	815	195	ND
W15	H. Ouled Yelles	47	7.1	1672	220	52	132	58	350	438	268	ND
W16	H. Ibainan	60	7.3	13,482	3660	81	112	496	5800	1500	372	ND
W17	H. Guerfa (Sedrata)	68	7.2	2206	95	16	118	380	250	900	366	53
W18	H. Ouled Ali (Guelma)	50	7	1140	30	8	62	166	40	438	372	50
W19	H. Sidi Trad (El Kala)	63	8	542	93	8	18	28	43	30	292	50

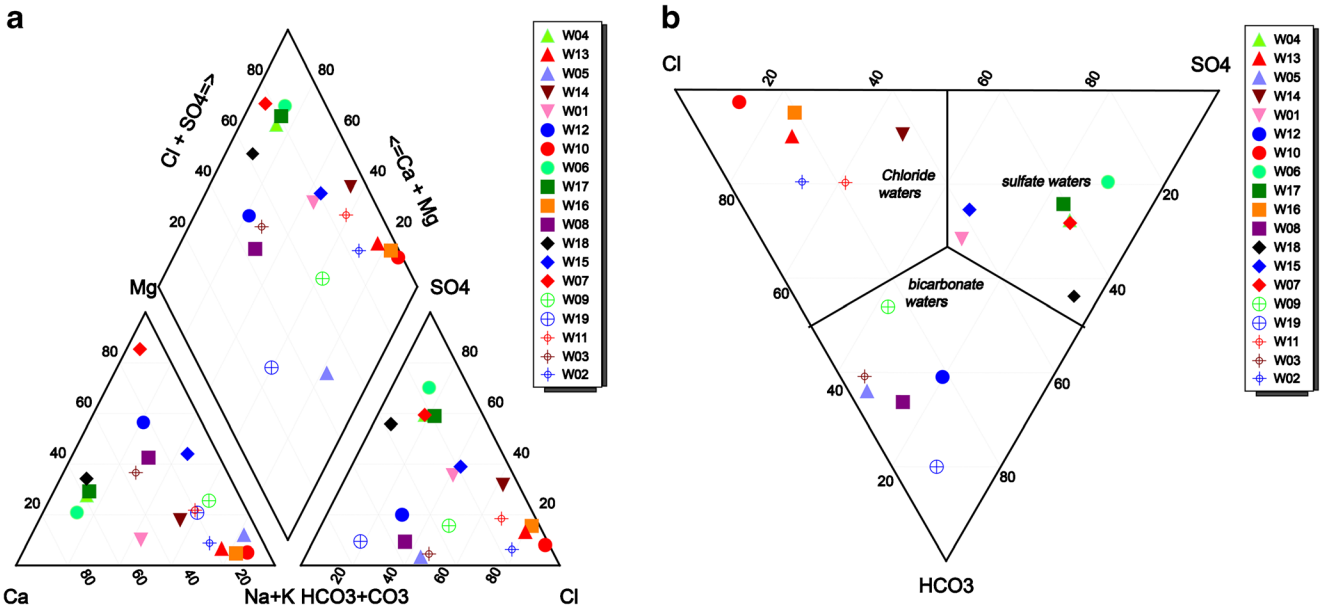

Fig. 4 **a** Piper diagram of northeastern hot spring samples (mg/L). **b** Ternary diagram of Cl-SO_4-HCO_3 showing the water types of the northeastern Algerian hot spring samples

W04, and W18 in Fig. 4a), even though it is creating a trend toward the chloride water corner, with higher Na-Cl species (W10, W16, W13, W02, W11, and W14 in Fig. 4b). The chemical composition and high TDS values of the water samples, which were obtained far away from seawater, reveal the evaporitic nature of the sedimentary host rocks, typically rich in gypsum and halite.

The third type is bicarbonate water, which is certainly rich in Ca-HCO_3 and Ca-Mg-HCO_3 (W12, W03, and W08 in Fig. 4a) and is poor in Na-HCO_3 contents prevailing (in W19 and W05 in Fig. 4a). This clearly reflects the interaction of meteoric water with the Jurassic age limestone and dolomite sequence, which constitute the principal reservoir rocks of the Tellian zones.

The Na and Cl contents are shown in the scatter diagram in Fig. 5a. The geothermal waters of the Tellian sector are strongly correlated with the halite dissolution line (R^2 = 0.94). Chlorides are known as highly mobile chemical species that interact weakly with the host rock (Herczeg and Edmunds 2000). Therefore, this correlation is likely explained by the enrichment of Na in Na-Cl waters from the interaction of the infiltrating water with the halite-bearing Triassic evaporites.

The Ca-SO_4 scatter diagram is shown in Fig. 5b. A typical SO_4-type composition can be identified for the geothermal waters of northeastern Algeria. Thus, several geothermal water samples from the Tellian zones are plotted along the gypsum dissolution line (W06, W17, W02, W11, W12, W04, and W10 in Fig. 5b), with a correlation coefficient of R^2 = 0.79. This result suggests that dissolution of sulfate minerals mainly hosted by the Triassic evaporitic sequence that controls the water chemistry of the Tellian zones.

Ca-Mg-HCO_3 and Na-HCO_3 waters are the significant type of the Tellian zones. They are generally located at depth with Cretaceous and Jurassic carbonate formations.

These geothermal waters have lower Ca/HCO_3 ratios (<1; W08, W19, W07, W12, W09, as shown in Fig. 5c) and correspond to the calcite dissolution line. Although calcite can precipitate as thermal water rises, this precipitation induces the depletion of HCO_3 in the thermal waters. Therefore, a higher Ca/HCO_3 ratio (>1) involves the contribution of Ca derived from the Triassic gypsum (W06, W16, W10, and W14 in Fig. 5c), which could be interpreted by the lack of deep water interaction with the shallower carbonate host rock during the ascension.

As shown in Fig. 5d, the key control processes of the northeastern geothermal waters indicate that Na and Cl contents are principally related to the dissolution of the saline Triassic formation, which is rich in halite (Iundt 1971; Edmunds et al. 2003).

Thus, the Na/Cl ratio of most of the geothermal water samples is buffered at ~1. However, the HCO_3/(SO_4+Ca) ratio indicates a much higher value that ranges between 1 and 10. Therefore, this dominant shift toward a greater value signifies calcite dissolution, which is typical for the Tellian carbonate units.

The higher Na/Cl ratio found in W19 and W05 in Fig. 5d may likely be due to Na percolation from sandstone and clay alteration of the Numidian flysch (Garcia et al. 2001; Fourré et al. 2011). Furthermore, the Na increase could also be supplied through the cation exchange process, with clays accompanied by Ca deficiency. This phenomenon has already been observed in circulating brines in sedimentary basins (Davisson and Criss 1996; Zilberbrand et al. 2001).

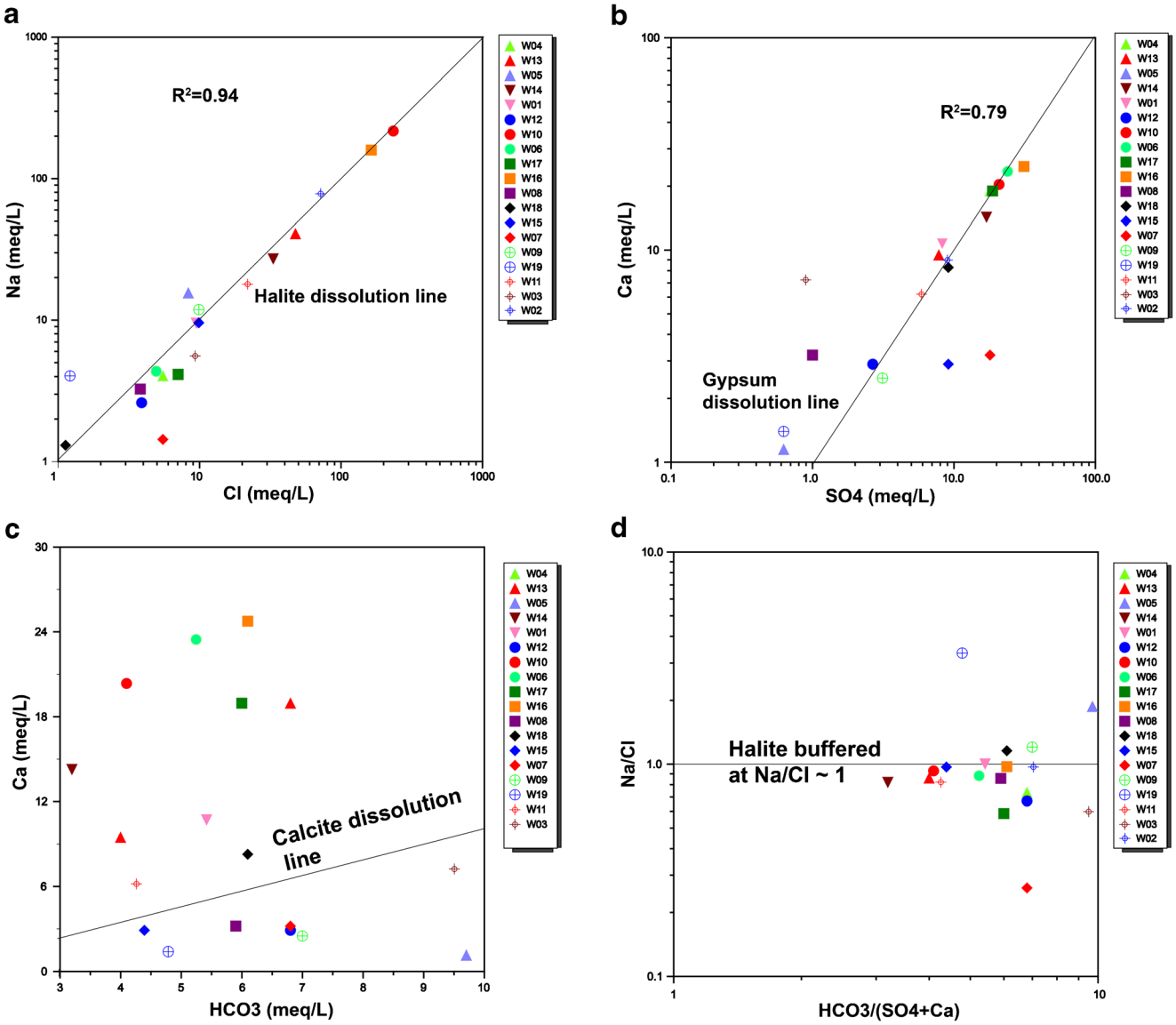

Fig. 5 **a** Na vs. Cl, **b** Ca vs. SO_4, and **c** Ca vs. HCO_3 scatter diagrams for the northeastern Algerian geothermal water samples, indicating the dissolution trends of halite, gypsum, and calcite. **d** Na/Cl vs. HCO_3/(Ca +SO_4) plots indicating the key source processes for the northeastern Algerian geothermal water samples

Na-K-Mg diagram

The ternary diagram of Na/1000-K/100-$Mg^{1/2}$ (Fig. 6) suggested by Giggenbach (1988) is used to estimate the reservoir temperatures.

At most, the northeastern Algerian geothermal water samples are plotted quite close to the $Mg^{1/2}$ corner, indicating an immature water field, except for samples W16 and W02 in Fig. 6. These samples fall in the equilibrated or mixed water field, providing temperatures of approximately 140 and 80 °C, respectively. Sample W10, as shown in Fig. 6, lies on the full equilibrium line and thus has a temperature of 40 °C due to the high Cl contents of ~8300 mg/L, which may have mixed with the original chloride fluid at depth.

The immature water plot of the thermal waters may result from the mixing of fully equilibrated or partly equilibrated geothermal waters with cold shallow and immature groundwaters rich in Mg contents. However, the use of such waters for evaluating geothermal reservoirs is dubious (Giggenbach 1988) because it makes the reliability of cationic geothermometers only tentative (Tarcan 2005).

Geothermometry

Solute geothermometers, which are mainly based on temperature-dependent mineral fluid equilibria, are known as valuable tools for evaluating geothermal reservoir temperatures. The following geothermometers were applied:

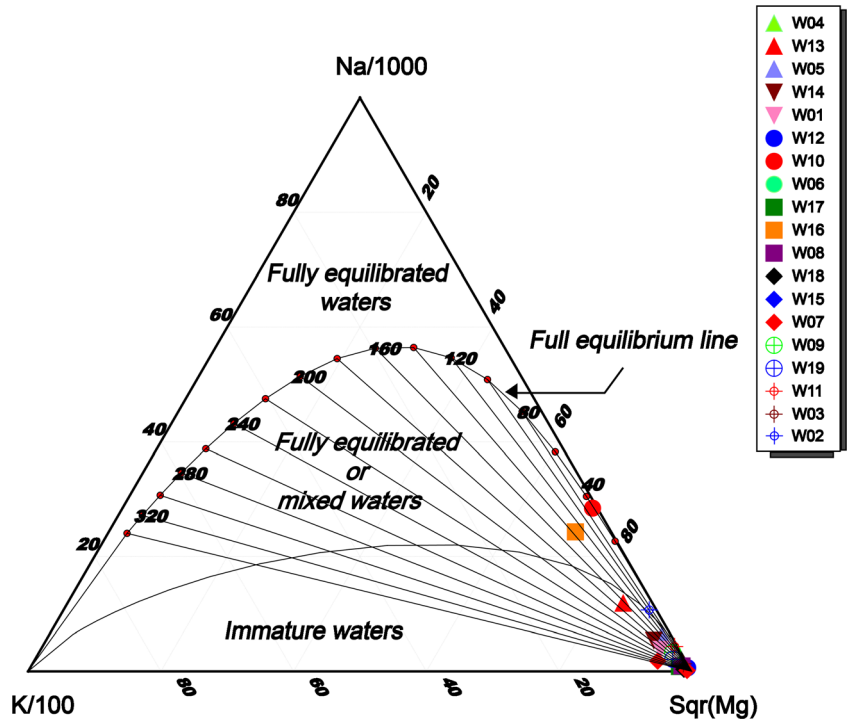

Fig. 6 Ternary Na-K-Mg diagram for the northeastern Algerian geothermal water samples (Giggenbach 1988)

(a) Na-K-Ca-Mg (Fournier and Potter 1979), (b) Na-K-Ca (Fournier and Truesdell 1973), (c) Na/K (Giggenbach 1988), (d) Na/K (Truesdell 1976), (e) Na/K (Tonani 1980), (f) Na/K (Nieva and Nieva 1987), (g) Na/K (Fournier 1979), (h) silica (Fournier and Potter 1982), (i) silica (Verma 2000), (j) cristobalite (α) (Fournier 1977), (k)

Table 2 Estimated temperatures (in °C) of the northeastern Algerian geothermal system using several cationic and silica geothermometers

Sample ID	Hot spring (prefecture)	a (°C)	b (°C)	c (°C)	d (°C)	e (°C)	f (°C)	g (°C)	h (°C)	i (°C)	j (°C)	k (°C)	l (°C)	m (°C)
W01	H. Chellala (Guelma)	214	111	209	156	188	179	192	122	118	71	101	133	93
W02	H. N'Bails (Guelma)	105	46	87	15	328	56	66	80	72	30	52	88	48
W03	H. Zaid	187	93	178	119	146	148	160	67	59	18	39	75	35
W04	H. Ben Hachani (Sedrata)	251	124	254	217	255	226	240	111	106	60	88	121	81
W05	H. Beni Salah (Guelma)	150	84	135	68	90	104	115	107	101	56	83	117	77
W06	H. El-Hamma	246	120	247	208	246	219	233	50	42	2	21	58	18
W07	H. Salhine (Skikda)	336	179	362	387	451	344	360	nd	nd	nd	nd	nd	nd
W08	H. Meksa (El Kala)	238	127	238	195	231	209	223	91	84	41	65	100	60
W09	H. Sidi Djaballah	175	95	163	100	125	132	144	84	77	34	57	92	52
W10	H. El Biban	68	23	48	nd	nd	18	26	nd	nd	nd	nd	nd	nd
W11	H. Soukhna	114	51	96	25	43	65	75	nd	nd	nd	nd	nd	nd
W12	H. El-Hamma-2	190	92	182	124	151	152	164	nd	nd	nd	nd	nd	nd
W13	H. Beni Haroune	176	95	164	101	127	133	145	nd	nd	nd	nd	nd	nd
W14	H. Boutaleb (Setif)	198	105	190	133	161	159	172	nd	nd	nd	nd	nd	nd
W15	H. Ouled Yelles	301	174	312	304	355	288	304	nd	nd	nd	nd	nd	nd
W16	H. Ibainan	150	80	135	68	90	103	115	nd	nd	nd	nd	nd	nd
W17	H. Guerfa (Sedrata)	272	136	277	252	295	252	266	104	99	54	81	115	75
W18	H. Ouled Ali (Guelma)	307	154	325	325	379	303	319	102	96	52	78	112	72
W19	H. Sidi Trad (El Kala)	224	125	221	172	205	191	205	102	96	52	78	112	72

(a) Na-K-Ca-Mg (Fournier and Potter 1979), $T = [1112/\log(\mathrm{Na/K}) + \beta \times \log(\mathrm{Ca/Na}) + 2.24] - 273.15$, $\beta = 1/3$ ast < 100 ° C, $R = \mathrm{Mg}/(\mathrm{Mg} + \mathrm{Ca} + \mathrm{K}) \times 100$ (Fournier and Potter 1979); (b) Na-K-Ca (Fournier and Truesdell 1973), $T = [1178/(\log(\mathrm{Na/K}) + 1.47) - 273]$, Mg % less than 8%, Mg % [100 Mg/TMEQ]; (c) Na/K (Giggenbach 1988), $T = [1217/(1.483 + \log(\mathrm{Na/K})] - 273.15$; (d) Na/K (Truesdell 1976), $T = [856/(0.857 + \log(\mathrm{Na/K})] - 273.15$; (e) Na/K (Tonani 1980), $T = [833/\log(\mathrm{Na/K}) + 0.780] - 273.15$; (f) Na/K (Nieva and Nieva 1987), $T = [1390/\log(\mathrm{Na/K}) + 1.75] - 273.15$; (g) Na/K (Fournier 1979), $T = [4410/14 - \log(\mathrm{K}^2/\mathrm{Mg})] - 273.15$; (h) silica (Fournier and Potter 1982), $T = [1175.7/4.8 - \log \mathrm{SiO_2}]$; (i) silica (Verma 2000), $T = [1032/(4.69 - \log \mathrm{SiO_2})] - 273.15$; (j) cristobalite (α) (Fournier 1977), $T = [1000/(4.55 - \log \mathrm{SiO_2})] - 273.15$; (k) silica (Giggenbach 1992), $T = [1309/(5.19 - \log C)] - 273.15$; (l) silica with no steam loss (Fournier 1977), $T = [42.198 + 0.278831C - 3.6686 \times 10^{-4} C^2 + 3.1665 \times C^3 + 77.034 \log C]$, where C is the $\mathrm{SiO_2}$ content in spring discharge; (m) chalcedony (Fournier 1992), $T = [1522/(5.75 - \log \mathrm{SiO_2})] - 273.15$

nd not determined

silica (Giggenbach 1992), (l) silica with no steam loss (Fournier 1977), and (m) chalcedony (Fournier 1992).

In the study area, the application of Na/K geothermometers provides high temperature results and a wide range for low-medium reservoir temperature. These wide-range temperatures are dependent of dissolution of Na^+ ions from halite mineral rather than chemical equilibrium at low temperatures (Haklidir 2013; Belhai et al. 2016). Therefore, they consistently provide reliable results if reservoir temperatures exceed 180°, with a minimum of 150 °C (Truesdell et al. 1987). They infer temperatures between 46 and 324 °C in W02 and between 136 to 295 °C in W17. In contrast, temperatures estimated by Na-K-Ca geothermometers (b) approximate those estimated by silica geothermometers (h) to (m), suggesting that Na-K-Ca is less affected by mixing with cold waters and precipitation of calcite causing the loss of Ca.

As shown in Table 2, reservoir temperatures were estimated by silica geothermometers (h) to (m), which can be more sensitive to mixing and fairly reflect a rapid reaction. Therefore, these geothermometers should be appropriate to be applied for geothermal waters of the study area. At temperatures less than 180 °C, the solubility of silica is often controlled by chalcedony rather than quartz, and in the dolomite-limestone reservoir such as the northeastern Algeria geothermal fields, it is important to apply quartz geothermometers cautiously, despite the fact that a chalcedony geothermometer infers temperatures approximating to the discharge temperature on-site. Consequently, the calculated reservoir temperatures by quartz geothermometers (h) and (i) shown in Table 2 and Fig. 7 infer values between 118 and 122 °C in W01 and between 106 and 111 °C in W04 and appear to be more valid than those calculated by the other geothermometers for the thermal waters in the study area because of the mixing process.

Gas chemistry

Table 3 shows the relative amounts of the major and noble gas components (N_2, O_2, CO_2, CH_4, H_2, H_2S, He, and Ar) in the dry gas phase at equilibrium for each geothermal

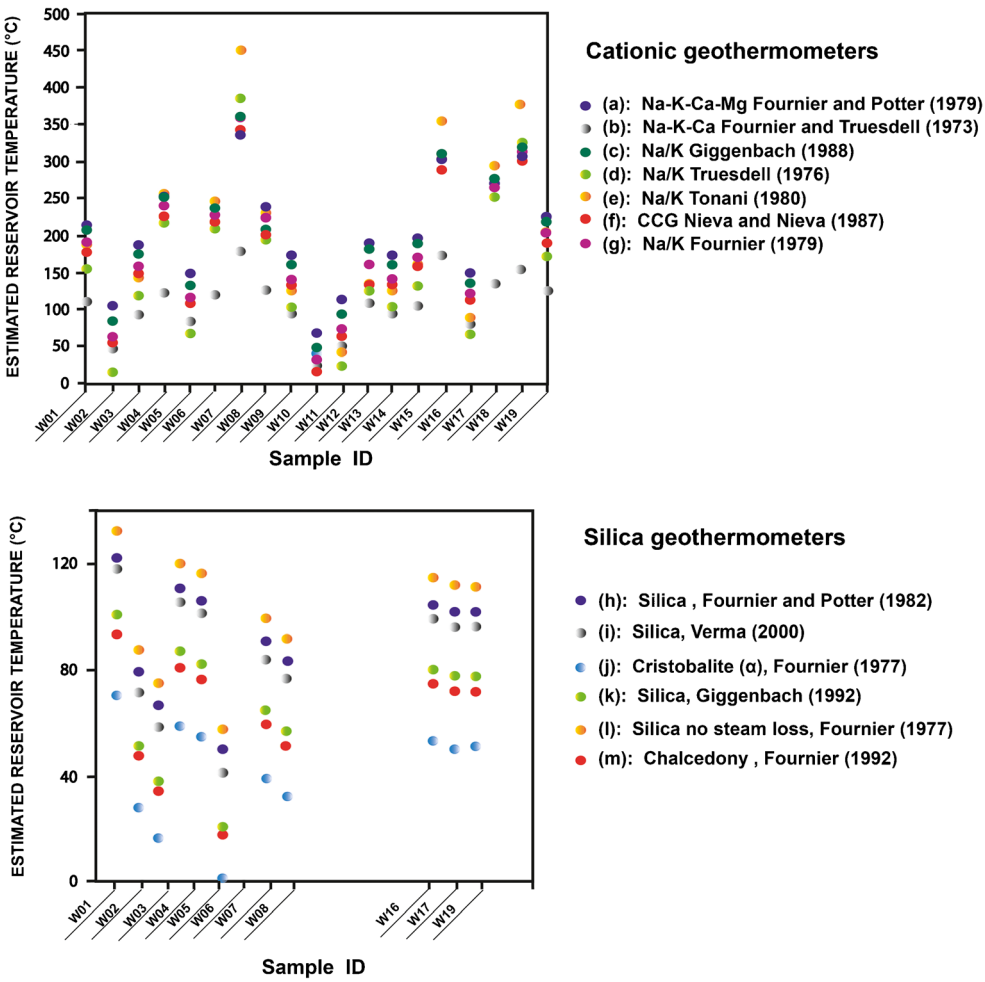

Fig. 7 Estimated reservoir temperatures based on different cationic geothermometers and silica geothermometers

water sample of northeastern Algeria (Rezig and Marty 1995). The gas dataset from northeastern Algeria indicates an excess of CO_2 and N_2, which involves the contribution of hydrothermal fluid from a deeper source, characterized by lower amounts of low-soluble species such as H_2 and CH_4, i.e., the N_2-He*1000-Ar*100 (a), N_2-CH_4-H_2S (b), and CH_4-H_2-H_2S (c) ternary mixing models of Werner et al. (2008) shown in Fig. 8.

The use of gas ratios in the northeastern Algerian geothermal water samples reveals the following:

- W07, W08, W10, W11, and W15 show a higher N_2/O_2 ratio, whereas W02, W09, W12, and W13 have values near those of air and have higher O_2 concentrations. However, these results likely reflect the air contamination by the enrichment of O_2 in the thermal water and indicate N_2/Ar ratios between 43.2 and 87.5, the latter of which is close to the contamination ratio (~84). The meteoric origin of thermal water generally indicates an N_2/Ar ratio of ~37, which is compatible with samples W01, W02, W05, and W08.
- The He/Ar ratio gives greater values than the atmospheric value of 5.7×10^{-4} (Nicholson 1993).
- W10 has a high He/Ar value of 0.213 and a low N_2/He value of 312.5. The high helium value could be explained by the high residence time or existence of a deep granitic intrusion *batholite numide* (Cormy and Demians d'Archimbaud 1970).

Helium isotopic composition

The $^3He/^4He$ ratio ranges from 0.04 Ra to 0.79 Ra (Table 3). These lower values of $^3He/^4He$ are compatible to the crustal source ratio (lower crust is assumed to have $^3He/^4He$ = 0.01 Ra; the upper crust has $^3He/^4He$ = 0.06 Ra; Italiano et al. 2014). $^4He/^{20}Ne$ falls between 0.4 and 159.8, thus revealing a mixture from the crust and atmosphere and, likely, the absence of mantle contribution.

The excess CO_2 and increase in H_2S correspond to the increase of the crustal gas component and contribute to the decrease of the $^3He/^4He$ ratio from 0.38 Ra to 0.04 Ra, which is compatible with crustal-derived helium.

However, a lower helium concentration could be explained by the depletion of mantle-derived helium from the reservoir via CO_2 oversaturation, accompanied by mixing with cold meteoric water or groundwater containing nearly radiogenic helium (Wiersberg et al. 2011).

The increase in N_2 in hot springs and the decrease of CO_2 in Table 3 give higher values of the $^3He/^4He$ ratio that were clearly above the crustal ratio and approached 1 Ra and lower $^4He/^{20}Ne$ ratios that were close to the air ratio of 0.285 (Mamyrin and Tolstikhin 1984) because of

Table 3 Chemical composition of 12 gas samples and helium isotopic composition (mmol/mol) of northeastern Algeria (Rezig and Marty 1995)

Sample ID	Station ID	*T* (°C)	CO_2	H_2S	CH_4	H_2	N_2	O_2	Ar	He	R/Ra	$^4He/^{20}Ne$	N_2/O_2	N_2/Ar	He/Ar	N_2/He
W01	H. Chellala	94.3	994.9	1.4	0.46	ND	4.1	0.11	0.11	0.0004	0.38	13.5	37.272	37.272	0.004	8913.043
W02	H. N'Bails	42.7	570.4	ND	ND	0.3	337	85	7.8	0.022	0.462	1.1	3.964	43.205	0.002	15,318.18
W04	H. Ben Hachani	71.7	774	9	9.7	0.035	204	ND	2.9	0.083	0.134	14.7	ND	70.344	0.028	2457.831
W05	H. Beni Salah	36.3	825	1.8	1.2	ND	167	ND	4.8	0.013	0.12	3	ND	34.791	0.002	12,846.15
W07	H. Salhine	48.1	39.6	0.039	0.054	0.017	680.9	0.039	9.84	0.08	0.21	1.5	17,459	69.197	0.008	8511.25
W08	H. Meksa	38	386.2	2.65	–	0.57	593.8	2.9	15.1	0.133	0.79	0.4	204.7	39.324	0.008	4464.662
W09	H. Sidi Djaballah	25.4	13.4	–	–	0.16	831.5	145	9.5	0.061	0.284	4.4	5.734	87.526	0.006	13,631.15
W10	H. El Biban	77.5	932	58	3.9	–	5	0.047	0.075	0.016	0.045	159.8	106.3	66.666	0.213	312.5
W11	H. Soukhna	46.4	31.2	ND	1.16	0.004	953	0.95	13	0.083	0.054	12.5	1003.1	73.307	0.006	11,481.93
W12	H. El-Hamma	35.7	484	ND	–	0.067	378	131	6.7	0.049	0.71	0.8	2.885	56.417	0.007	7714.286
W13	H. Beni Haroune	41.1	60.6	1.05	ND	–	874.7	52.4	11.1	0.108	0.225	10.8	16.692	78.801	0.009	8099.074
W15	H. Ouled Yelles	48.4	34.1	7.2	1.6	0.168	934.5	11	11.4	0.895	0.044	83.2	84.954	81.973	0.078	1044.134

H Hammam, *ND* not determined

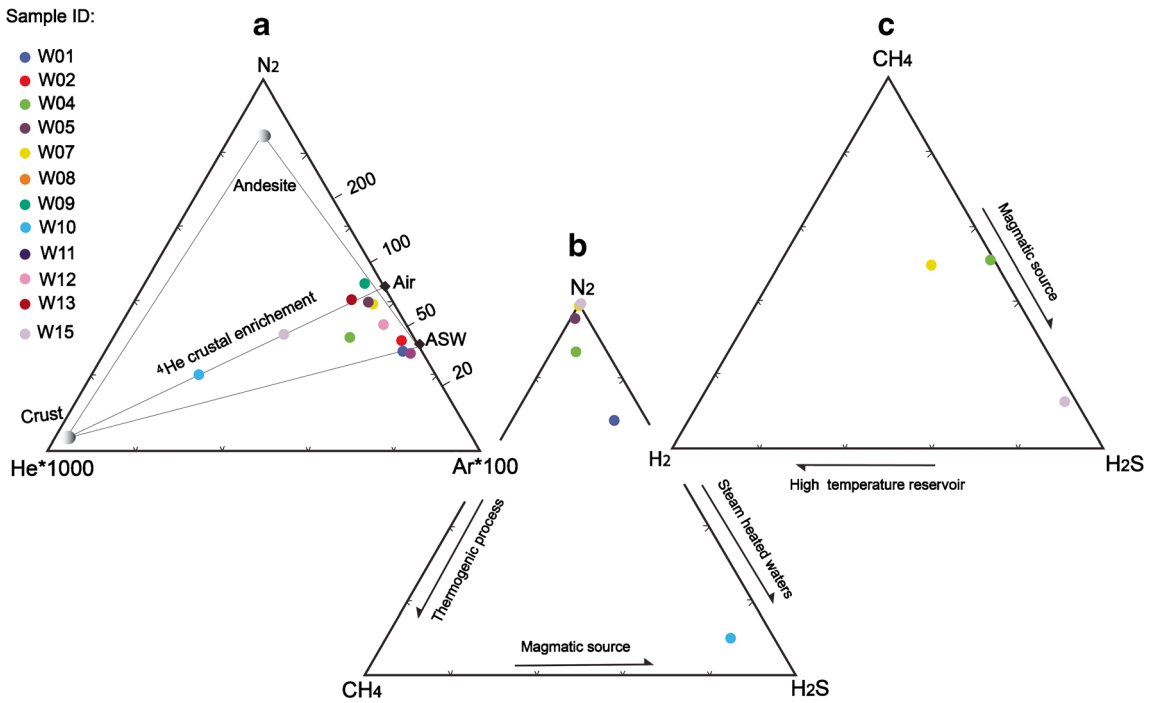

Fig. 8 **a** N_2-He*1000-Ar*100, **b** N_2-CH_4-H_2S, and **c** CH_4-H_2-H_2S ternary mixing models of the northeastern Algerian geothermal water. *ASW* air-saturated water

the higher sensitivity of Ne isotopes to atmospheric contamination, which is more abundant in the atmosphere than He (W08, W12, W02, and W07 in Fig. 9). However, the increase in N_2 and the low $^4He/^{20}Ne$ values indicate a probable atmospheric contribution by contamination.

Higher values of $^4He/^{20}Ne$ were recorded for samples W15 and W10, which are obviously explained by the existence of the batholite numide, as shown by Cormy and Demians d'Archimbaud (1970).

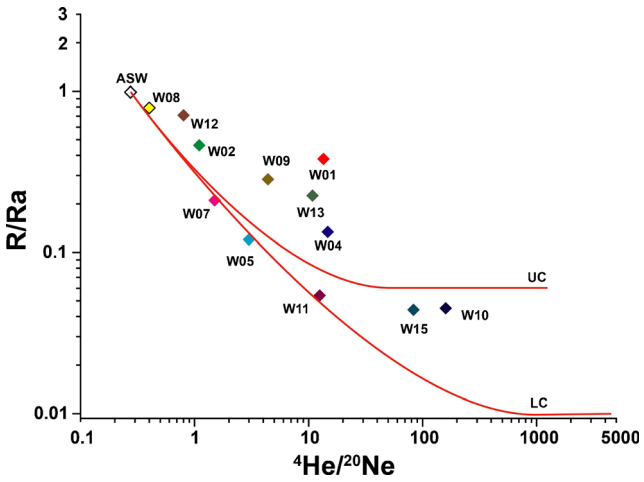

Fig. 9 Helium isotopic results plotted as R/Ra vs. $^4He/^{20}Ne$ for the northeastern Algerian hot springs. *Colored lines* show mixing trends between the atmospheric and crustal components

Gas geothermometry

The gas concentration in a geothermal reservoir is eventually affected by the gas ratio. However, the use of gas-gas geothermometers is needed to estimate the geothermal reservoir.

To better estimate the reservoir temperatures of the northeastern Algerian geothermal waters, four geothermometers, including CO_2-H_2S-CH_4-H_2 (D'Amore and Panichi 1980), H_2-Ar (Giggenbach and Goguel 1989), and CO_2-Ar and CO_2-H_2 (Giggenbach 1991), were applied in Fig. 10.

CO_2-H_2S-CH_4-H_2 (D'Amore and Panichi 1980) is partially empirical with respect to the selection of CO_2 partial pressure (P_{CO_2}), which is related to the proportion of CO_2 in the total gas content of the discharge (if $CO_2 < 75\%$, $P_{CO_2} = 0.1$; if $CO_2 > 75\%$, $P_{CO_2} = 1.0$; if $CO_2 > 75\%$, $CH_4 > 2H_2$, and $H_2S > 2H_2$, $P_{CO_2} = 10$). Therefore, the reservoir temperatures estimated using these geothermometers range between 161 and 313 °C, respectively (W04, W07, and W15 in Fig. 10a), with $P_{CO_2} = 0.1$ (Table 4). Those estimated temperatures are considered slightly higher than the reservoir temperatures because of the high CO_2 content in water due to the precipitation of carbonate minerals around the hot spring area.

The H_2-Ar geothermometer of Giggenbach and Goguel (1989) produces much lower estimated temperatures than the reservoir temperatures of the northeastern Algerian geothermal water (W02, W04, W08, W09, W12, and W15 in Fig. 10a). This is likely due to the low H_2 content compared with the other gas species, the consummation of H_2 due to the

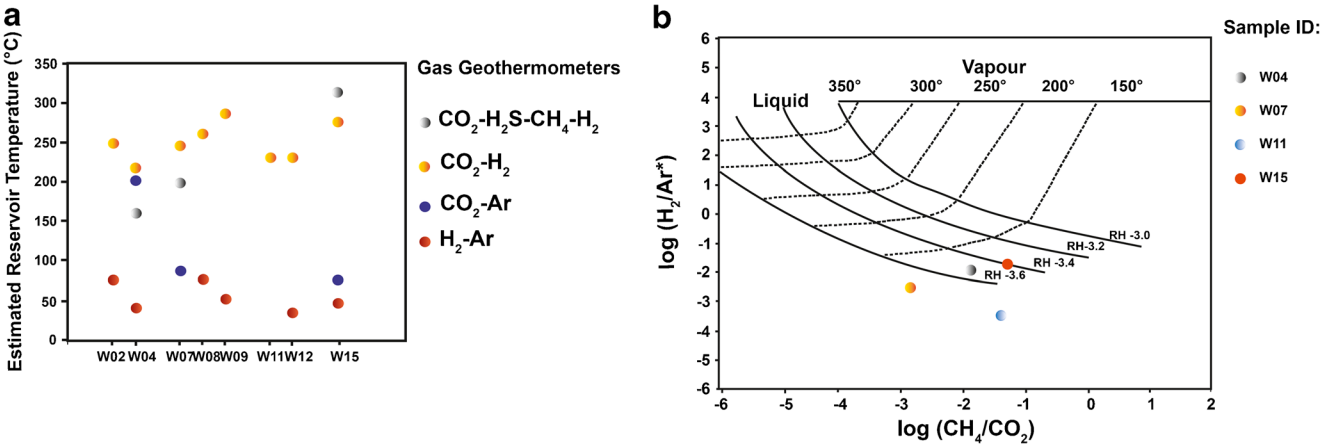

Fig. 10 **a**, **b** Estimation of reservoir temperatures using several gas geothermometers. CO_2-H_2S-CH_4-H_2: t (°C) = [24,775/(2log(CH_4/CO_2)−6log (H_2/CO_2) −3log (H_2S/CO_2) + 7logP_{CO_2} + 36.05)]−273 (D'Amore and Panichi 1980). H_2-Ar: t (°C) = 70 [2.5 + log(X_{H_2}/X_{Ar})] (Giggenbach and Goguel 1989). CO_2-Ar: t (°C) = [0.227 × t − 7.53 + 2048/t + 273]. CO_2-H_2: t (°C) = − 28.57 × log [CO_2/H_2] + 341.7 (Giggenbach 1991)

oxidation of pyrite to produce magnetite (Eq. 1), or alteration of the evaporite minerals, such as anhydrite in veins near the upflow area of W15. The effect of the dilution process in the geothermal water is far from negligible because dilution with meteoric recharge can increase Ar content and air contamination. However, this effect is less prominent when applying the CO_2-Ar geothermometer (Giggenbach 1991).

$$3FeS_2 + 2H_2 + 4H_2O = Fe_3O_4 + 6H_2S \quad (1)$$

Furthermore, the CO_2-H_2 geothermometer (Giggenbach 1991) estimated higher temperatures, ranging between 217 and 275 °C (W02, W04, W07, W08, W09, W11, W12, and W15 in Fig. 10a). These results likely reflect the depletion of H_2 and the carbonated nature of the hot rock, which leads to the precipitation of calcite and the increased CO_2 in the water.

Figure 10b shows the CH_4/CO_2 vs. H_2/Ar* diagram, in which Ar* = Ar − (O_2/22) is used to avoid atmospheric contamination at the ground surface in the absence of O_2. The samples (W04, W07, W11, and W15 in Fig. 10b) give lower temperatures than 150 °C, and $-3.6 \le R_H \le -3.4$ (R_H = logH_2/H_2O), which explains the equilibrium line at different temperatures of redox conditions. These results indicate that the fluid reservoir is of lower temperature due to the lower H_2 compared with other gas species. This

Table 4 Estimation of the geothermal reservoir temperature inferred on the basis of gas geothermometry and gas/gas ratios

Sample ID	H_2/Ar	CO_2/H_2	CO_2/Ar	CH_4/Ar	CO_2/H_2S	I (°C)	II (°C)	III (°C)	IV (°C)	P_{CO_2} (bar)
W01	–	–	9044.5	4.1818	710.643	ND	ND	ND	ND	0.1
W02	0.038	1901.3	73.1	ND	ND	–	248	ND	77	10
W04	0.012	22,114.3	266.8	3.3	86	161	217	204	41	0.1
W05	–	ND	171.8	0.25	458.333	–	–	–	–	0.1
W07	0.001	2329.4	4.02	0.005	1015.38	199	245	90	–	0.1
W08	0.037	677.5	25.57	ND	145.736	–	260	–	77	0.1
W09	0.016	83.7	1.41	ND	ND	–	286		52	0.1
W10	–	–	12,426.67	52	16.069	–	–	–	–	0.1
W11	0.0003	7800	2.4	0.08	ND	–	230	–	–	0.1
W12	0.01	7223.8	72.23	ND	ND	–	231	–	35	0.1
W13	–	ND	5.45	ND	57.714	–	–	–	–	0.1
W15	0.014	202.9	2.99	0.141	4.7361	313	275	79	47	0.1

I (°C): CO_2-H_2S-CH_4-H_2 (D'Amore and Panichi 1980); II (°C): CO_2-H_2 geothermometer (Giggenbach 1991); III (°C): CO_2-Ar geothermometer (Giggenbach 1991); IV (°C): H_2-Ar Giggenbach and Goguel (1989)

ND not determined

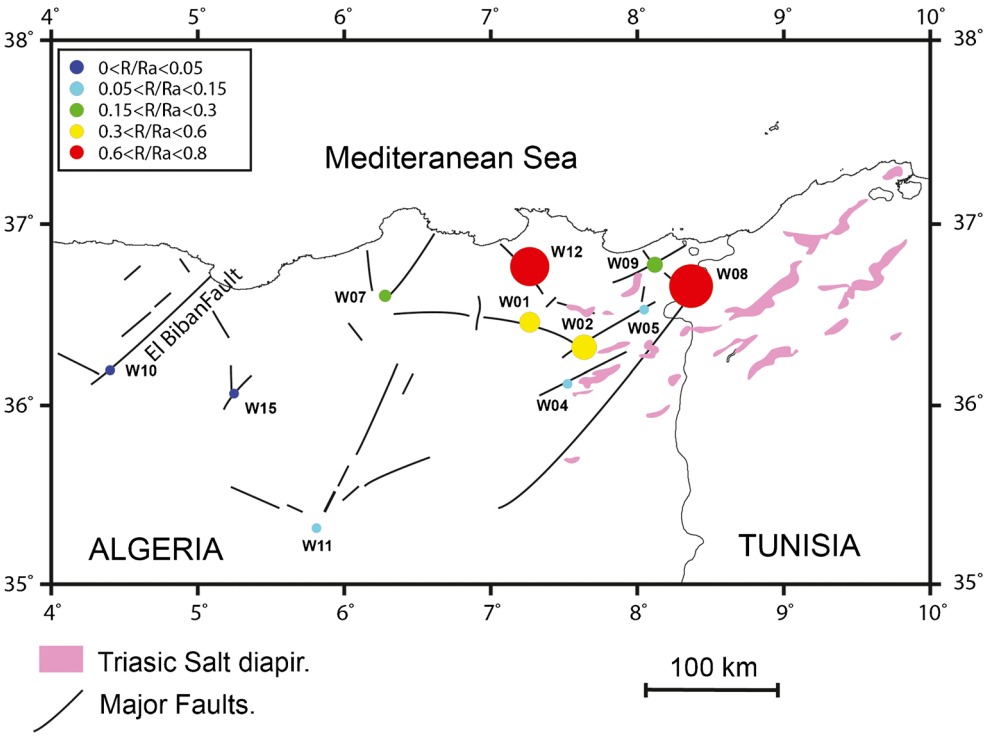

Fig. 11 Map of the spatial distribution of R/Ra in northeastern Algeria and its connection with major faults

shift toward lower temperatures likely reflects a larger contribution of vapors that are either relatively depleted in H_2 by boiling or enriched in Ar, possibly related to meteoric recharge.

The probable presence of secondary dissolution, such as Triassic anhydrite, produced by fluid-rock redox causes the consummation of H_2, which can affect the calculated equilibrium temperature (Joseph et al. 2011; Magro et al. 2013). The resultant H_2S of the rising gas could be promptly oxidized in the interaction with cold ground water and could lead to sulfate waters with higher SO_4 content (Cinti et al. 2014).

Origin of helium and the link with tectonic activity

Helium isotopes are considered powerful indicators of the origin of volatiles and susceptible tracers of the mantle-derived contribution to crustal fluids (Ballentine et al. 2002; Jean-Baptiste et al. 2014). In northeastern Algeria, the crustal radiogenic helium composition is the most dominant in all geothermal samples. This could typically be related to the geodynamical context of the Tellian sector.

The lowest value ranges between 0 Ra and 0.04 Ra, associated with high SO_4 content, and deep Cl waters (see W10 and W15 in Fig. 11) are compatible with crustal ratios with no detectable amount of mantle-derived ^3He in the geothermal water.

These results indicate that the helium isotopic composition in the sedimentary basin is impermeable to mantle volatiles (Marty et al. 2003; Fourré et al. 2011). Helium values of 0.05 to 0.15 (see W04, W05, and W11 in Fig. 11) remain close to the crustal ratio. The high ^4He is likely due to subsurface feeding of the crustal flux along large-scale faults, such as the NE-SW El Biban Fault and the E-W Debbagh Fault.

Toward the extreme northeastern part of Algeria, the $^3He/^4He$ ratio spatially increases up to 0.8 Ra, which is accompanied by a

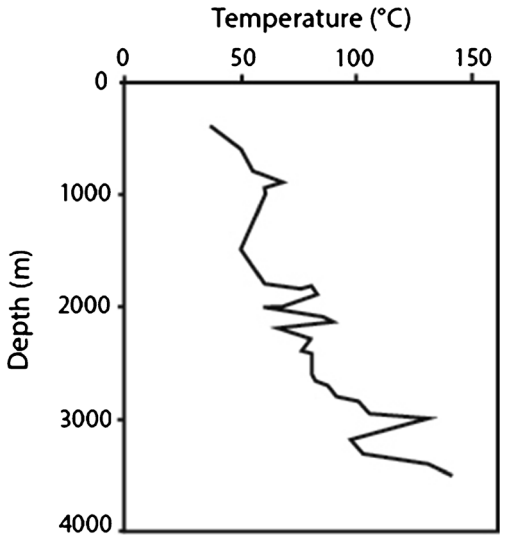

Fig. 12 Downhole measured temperature of the petroleum well ZM1 (Rezig 1991)

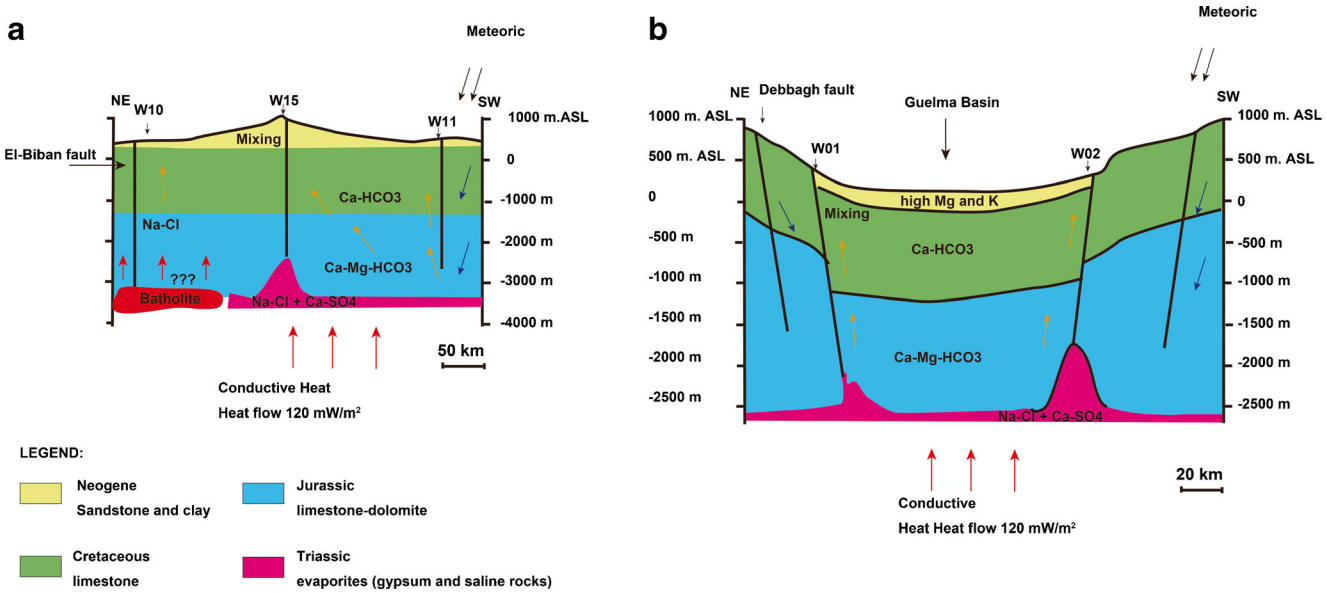

Fig. 13 Geothermal conceptual models of northeastern Algeria. **a** Geothermal conceptual model of Hammam El Biban (W10). **b** Geothermal conceptual model of the hot springs in the Guelma Basin

minor mantle-derived helium composition when $^3He/^4He$ ~0.6 (see W08 and W12 in Fig. 11). This is probably linked to the significant seismic activity characterizing the study area (Fourré et al. 2011; Maouche et al. 2013) and may lead to mantle-derived helium release along the deep NE-SW and E-W active faults.

Another possible reason of northward ^3He enrichment is melting at the depth of the recent mantle, as indicated by the localization of eruptive and granitic rocks in the coastal zones, which range between 9.3 and 24.4 Ma in age (Rezig and Marty 1995). This effect is less expressed in the south, which suggests the placement of the plutonic source at depth (Maouche et al. 2013).

Conceptual model

A conceptual model was proposed by Saibi (2009), who suggested a location of conductive heat at a penetration depth of 7 km in northeastern Algeria. In contrast, Cormy and Demians d'Archimbaud (1970) suggested the presence of a batholite intrusion.

The penetration depth of the water in the northeastern geothermal system of Algeria is approximately 2.5 km, as calculated from the estimated reservoir temperature using silica geothermometers.

The temperature profile for the 4000-m-deep petroleum well ZM1 (Fig. 12) is located near W15, W11, and W10. The well data reveal the presence of two anomalies at depths of 2 and 3 km. The geothermal reservoir could explain the 2-km-depth temperature anomaly, whereas the 3-km-depth temperature anomaly could be related to the batholite intrusion proposed by previous studies (Fig. 13).

Discussion and conclusions

The chemical composition of the thermal waters in northeastern Algeria is a function of the local tectonic setting and variable geological features. Thus, halite and gypsum dissolution from the Triassic evaporites strongly influences the chemistry of the hot springs. Few samples have recorded radiogenic helium associated with higher CO_2 of biogenic origin (Issaadi 1992) induced by calcite precipitation from shallower carbonate rocks of the Tellian sector. Higher H_2S content accompanied this CO_2 excess and resulted from the consummation of H_2 from boiling and separation, which caused a lower reservoir temperature (<150 °C) and likely produced a similar result to the silica geothermometers that easily reach equilibrium in cases of immature water types, such as those in northeastern Algeria. This is likely due to the leaching of Mg when the thermal water rises to the ground surface. In fact, the effect of dilution with cold groundwater or meteoric water increases the amounts of N_2 and Ar resulting from the contamination.

Those higher amounts correspond to the increase of the $^3He/^4He$ ratio and the lower $^4He/^{20}Ne$ ratio due the high abundance of Ne in the atmosphere. The suggested existence of a batholite intrusion in the El Biban region is well correlated with the high He/Ar ratio of 0.213. The lower $^3He/^4He$ ratio and the higher $^4He/^{20}Ne$ ratio correspond to continental crust values. The increase in mantle-derived ^3He is logically explained by the seismic activity in northern Algeria and the development of a deep fractured zone, which has led to the release of mantle-derived helium.

The conceptual model suggests that the northeastern Algerian geothermal system was developed by the deep

penetration of infiltrated cold groundwaters to a depth of up to 2.5 km and then heated by a conductive heat source (the batholite in the El Biban case). The hot water flowed to the surface through the deep-seated fractures. During its ascension, the hot waters mixed with shallow cold groundwaters, thereby increasing the Mg contents and causing the immature classification of the hot water samples.

Acknowledgements The first author would like to express his sincere thankful acknowledgements to Ms. Messaouda Rezig from the Research Center of Renewable Energy (CDER), Algiers, Algeria, for supplying the essential documentation and material on the hot springs investigated in this study. Finally, we thank the anonymous reviewers for their fruitful comments to enhance this research.

References

Auboin J, Durand-Delga M (1971) Aire mediterraneenne. Encyclopidia universalis 10:743–745

Ballentine CJ, Burgess R, Marty B (2002) Tracing fluid origin, transport and interaction in the crust. In: Porcelli D, Ballentine CJ, Wieler R (eds) Noble gases in geochemistry and cosmochemistry. Rev Mineral Geochem 47:539–614

Belhai M, Fujimitsu Y, Bouchareb-Haouchine FZ, Haouchine A, Nishijima J (2016) A hydrochemical study of the Hammam Righa geothermal waters in north-central Algeria. Acta Geochemica 35(3): 271–228

Bouchareb-Haouchine FZ (1993) Apport de la géothermométrie et des données de forages profonds à l'identification des ressources géothermiques de l'Algérie du Nord. Application à la région du Hodna. Mémoire de Magister, Univ. Alger, Algérie, 105p

Bouchareb-Haouchine FZ (2012) Etude Hydrochimique des Sources Thermales de l'Algérie du Nord- Potentialités Géothermiques. These Doctorat en Sciences, USTHB, Algiers, p. 135

Cermak V, Rybach L (1982) Thermal conductivity and specific heat of minerals and rocks. In: Angenheister G (ed) Landolt-Börnstein: numerical data and functional relationships in science and technology, new series, group V (geophysics and space research), Voi. 1a (physical properties of rocks). Springer, Berlin, pp. 305–343

Cinti D, Tassi F, Procesi M, Bonini M, Capecchiacci F, Voltattorni N, Vaselli O, Quattrocchi F (2014) Fluid geochemistry and geothermometry in the unexploited geothermal field of the Vicano–Cimino Volcanic District (Central Italy). Chem Geol 371:96–114

Cormy G, Demians d'Archimbaud J (1970) Les possibilités géothermiques de l'Algérie. Geothermics 2:110–116

D'Amore F, Panichi C (1980) Evaluation of deep temperatures of hydrothermal systems by a new gas-geothermometer. Geochim Cosmochim Acta 44:549–556

Davisson ML, Criss RE (1996) Na-Ca-Cl relations in basinal fluids. Geochimica Cosmochimica Acta 60:2743–2752

Domzig A, Yelles A-K, Le Roy C, Déverchère J, Bouillin J-P, Bracene R, Mercier de Lépinay B, Le Roy P, Calais E, Kherroubi A, Gaullier V, Savoye B, Pauc H (2006) Searching for the Africa–Eurasia Miocène boundary offshore western Algeria (MARADJA'03 cruise). C R Geosci 338:80–91

Durand-Delga M (1969) Essai sur la structure du NE de la Berberie. Bull Serv Carte geol Algérie 39:89–181

Edmunds WM, Guendouz AH, Mamou A, Moula A, Shand P, Zouari K (2003) Groundwater evolution in the Continental Intercalaire aquifer of southern Algeria and Tunisia: trace element and isotopic indicators. Appl Geochem 18:805–822

ENEL (1982) Etude de reconnaissance geothermique du Constantinois oriental. Internal report SONELGAZ, 135 pp

Fournier RO (1977) Chemical geothermometers and mixing models for geothermal systems. Geothermics 5:41–50

Fournier RO (1979) Geochemical and hydrologic considerations and the use of enthalpy–chloride diagrams in the prediction of underground conditions in hot spring systems. J Volcanol Geotherm Res 5:1–6

Fournier RO (1992) Water geothermometers applied to geothermal energy. In: D'Amore F (Coordinator) Application of geochemistry in geothermal reservoir development. UNITAR/UNDP, Vial del Corso, Italy, pp. 37–69

Fournier RO, Potter RW (1979) Magnesium correction to the Na–K–Ca chemical geothermometer. Geochim Cosmochim Acta 43:1543–1550

Fournier RO, Potter RW (1982) A revised and expanded silica (quartz) geothermometer. Geoth Res Council Bull, November, 3–12

Fournier RO, Truesdell AH (1973) An empirical Na–K–Ca geothermometer for natural waters. Geochim Cosmochim Acta 37:1255–1275

Fourré E, Di Napoli R, Aiuppa A, Parello F, Gaubi E, Jean-Baptiste P, Allard P, Calabrese S, Ben Mamou A (2011) Regional variations in the chemical and helium–carbon isotope composition of geothermal fluids across Tunisia. Chem Geol 288:67–85

Garcia MG, Del Hidalgo M, Blesa MA (2001) Geochemistry of groundwater in the alluvial plain of Tucuman province Argentina. J Hydrol 9:597–610

Giggenbach WF (1988) Geothermal solute equilibria. Derivation of Na-K-mg-Ca geoindicators. Geochim Cosmochim Acta 52:2749–2765

Giggenbach WF (1991) Chemical techniques in geothermal exploration. Applications of geochemistry in geothermal reservoir development series of technical guides on the use of geothermal energy, by Franco D'Amore, pp. 119–142

Giggenbach WF (1992) Isotopic composition of geothermal water and steam discharges. In: D'Amore F (Coordinator) Application of geochemistry in geothermal reservoir development. UNITAR/UNDP, Vial del Corso, Italy, pp. 253–273

Giggenbach WF, Goguel RL (1989) Collection and analysis of geothermal and volcanic water and gas discharges, Report No. CD 24014th ed. DSIR, New Zealand, p. 81

Gouskov N, Laffitte R (1951) Carte géologique de l'Algérie 1:500,000. Constantine sud Algeria. Service de la carte géologique de l'Algérie. Société nationale de recherche et d'exploitation des pétroles en Algérie

Guiraud R (1970) Sur la présence de décrochements dextres d'orientation E-W dans l atlas saharien. interpretation magmatique. *C.R.S.S.G.F.,* FASC.8:316

Haklidir FT (2013) Hydrogeochemical evaluation of thermal, mineral and cold waters between Bursa city and Mount Uludag in the South Marmara region of Turkey. Geothermics 48:132–145

Herczeg AL, Edmunds WM (2000) Inorganic ions as tracers. In: Cook PG, Herczeg AL (eds) Environmental tracers in subsurface hydrology. Kluwer Academic, Glen Osmond, pp. 31–77

Issaadi A (1992) Le Thermalisme dans son Cadre Geostructural, Apport a la connaissance de la structure profonde de l'Algérie et de ses Ressources Geothermales. These Doctorat d'Etat., Univ.Sci.et Tech., Alger

Italiano F, Yuce G, Uysal IT, Gasparon M, Morelli G (2014) Insights into mantle-type volatiles contribution from dissolved gases in artesian waters of the Great Artesian Basin, Australia. Chem Geol 378–379:75–88

Iundt F (1971) Potentiel géothermique de la Tunisie. Etude géochimique. Bureau de Recherches Géologiques et Minières. Service Géologique National, Orléans, France

Jean-Baptiste P, Allard P, Fourré E, Parello F, Aiuppa A (2014) Helium isotope systematics of volcanic gases and thermal waters of Guadeloupe Island, Lesser Antilles. J Volcanol Geotherm Res 283:66–72

Joseph EP, Fournier N, Lindsay J, Fischer T (2011) Gas and water geochemistry of geothermal systems in Dominica, Lesser Antilles island arc. J Volcanol Geotherm Res 206:1–14

Kedaid F-Z (2007) Database on the geothermal resources of Algeria. Geothermics 36:265–275

Kedaid F-Z, Mesbah M (1996) Geochemical approach to the Bou Hadjar hydrothermal system (NE Algeria). Geothermics 25:249–257

Lerche I, O'Brien J (1987) Dynamical geology of salt and related structures. Academic Press, Orlando, pp 163–259

Magri F, Littke R, Rodon S, Bayer U, Urai J L (2008). Temperature fields, petroleum maturation and fluid flow in the vicinity of salt domes. Dynamics of complex intracontinental basins—The Central European Basin System: Springer-Verlag, Berlin, pp 323–330

Magro G, Gherardi F, Bayon FEB (2013) Noble and reactive gases of Palinpinon geothermal field (Philippines): origin, reservoir processes and geodynamic implications. Chem Geol 339:4–15

Mamyrin BA, Tolstikhin IN (1984) Helium isotopes in nature. Elsevier, New York

Maouche S, Abtout A, Merabet N, Aïfa T, Lamali A, Bouyahiaoui B, Bougchiche S, Ayache M (2013) Tectonic and hydrothermal activities in Debagh, Guelma Basin (Algeria). J Geol Res 2013, Article ID 409475. 13 pages

Marty B, Dewonck S, France-Lanord C (2003) Geochemical evidence for efficient aquifer isolation over geological timeframes. Nature 425:55–58

Nicholson KN (1993) Geothermal fluids. Chemistry and exploration techniques, xv + 263 p

Nieva D, Nieva R (1987) Development in geothermal energy in Mexico, part 12—a cationic composition geothermometer for prospection of geothermal resources. Heat Recover Syst CHP 7:243–258

Rezig M (1991) Etude geothermique du Nord Est de l'Algerie. Memoire de DEA, Tectonique-Géophysique. Géochimie–Hydrogéol.[T.G.G.H]. Université de Monpellier 2, France, p. 58

Rezig M, Marty B (1995) Geothermal study of the northeastern part of Algeria. Proceedings of the World Geothermal Congress, vol. 2, Florence, Italy, pp. 1151–1155

Saibi H (2009) Geothermal resources in Algeria. Renew Sust Energ Rev 13:2544–2552

Tarcan G (2005) Mineral saturation and scaling tendencies of waters discharged from wells (>150 °C) in geothermal areas of Turkey. J Volcanol Geotherm Res 142:263–283

Tonani F (1980) Some remarks on the application of geochemical techniques in geothermal exploration. In: Proc. Adv. Eur. Geoth. Res., Second Symposium, Strasbourg, pp. 428–443

Truesdell AH (1976) Summary of section III. Geochemical techniques in exploration. Proceeding 2nd UN symposium on the development and use of geothermal resources, San Francisco, 1975, 1, liii-lxxix

Truesdell AH, Winnett TL, Nieva D, Barragan RM, Ramirez E, (1987). Chemical modeling of geothermal aquifer fluids with sample calculations for Los Azufres and Cerro Prieto. In: Proceedings of International Symposium On Development and Exploitation of Geothermal Resources, Cuernavaca, Mor., Mexico, pp. 194–201

Verdeil P (1982) Algerian thermalism in its geostructural setting. How hydrogeology has helped in the elucidation of Algeria's deep seated structure. J Hydrol 56:107–117

Verma MP (2000) Revised quartz solubility temperature dependence equation along the water–vapor saturation curve. In: Proceedings of the 2000. World Geothermal Congress, 28 May–19 June, Kyushu and Tohoku, Japan, pp. 1927–1932

Werner C, Hurwitz S, Evans WC, Lowenstern JB, Bergfeld D, Heasler H, Jaworowski C, Hunt A (2008) Volatile emissions and gas geochemistry of Hot Spring Basin, Yellowstone National Park, USA. J Volcanol Geotherm Res 178:751–762

Wiersberg T, Süer S, Güleç N, Erzinger J, Parlaktuna M (2011) Noble gas isotopes and the chemical composition of geothermal gases from the eastern part of the Büyük Menderes Graben (Turkey). J Volcanol Geotherm Res 208:112–121

Wildi W (1983) La chaine tello-rifaine. Structure, stratigraphie et évolution du Trias au Miocène. Rev Geol Dyn et geogr Phys 24:201–297

Zilberbrand M, Rosenthal E, Shachnai E (2001) Impact of urbanization on hydrochemical evolution of groundwater and on unsaturated-zone gas composition in the Coastal City of Tel Aviv, Israel. J Contam Hydrol 50:175–208